

Article

Preparation and Selection of Best-Performing Fluorescent-Based Tracers for Oil and Gas Downhole Applications

Vladimir Khmelnitskiy ¹, Nouf AlJabri ² and Vera Solovyeva ^{1,*} ¹ Aramco Innovations, bld.1-75B, Leninskiye Gory, 119234 Moscow, Russia² Saudi Aramco Research Center at KAUST, Thuwal 23955, Saudi Arabia

* Correspondence: vera.solovyeva@aramcoinnovations.com

Abstract: Cost-efficient tracers with fast and simple detection and quantification methods at low detection limits via on-site detection is a current industrial target for state-of-the-art tracer tests. To bridge the gap between the desired tracer properties and detection limits, we developed a broad spectrum of robust and cost-efficient fluorescent tags to innovate the current reservoir management practices. We engineered new tracers and extended tracer test applications for on-site real-time well-drilling monitoring to label drill cuttings as they are made at the drill-bit face to improve drill-cuttings depth correlation. These developed fluorescent tracers not only have the low detection limits of fluorescent spectroscopy techniques but also allow for automated detection at minimal concentrations of 0.025–0.037 mol.%. These developed tracers allow us to detect the real-time drilling depth, thereby enhancing hydrocarbon recovery. Thus, the reported innovative fluorescent-based tracing approach would (1) reduce drilling depth correlation uncertainty, (2) optimize well placement, and (3) maximize oil production.

Keywords: fluorescence-loaded tracers; drill-cuttings labeling; drilling depth determination; reservoir characterization



Citation: Khmelnitskiy, V.; AlJabri, N.; Solovyeva, V. Preparation and Selection of Best-Performing Fluorescent-Based Tracers for Oil and Gas Downhole Applications. *Processes* **2022**, *10*, 1741. <https://doi.org/10.3390/pr10091741>

Academic Editor: Anil K. Bhowmick

Received: 3 August 2022

Accepted: 29 August 2022

Published: 1 September 2022

Publisher's Note: MDPI stays neutral with regard to jurisdictional claims in published maps and institutional affiliations.



Copyright: © 2022 by the authors. Licensee MDPI, Basel, Switzerland. This article is an open access article distributed under the terms and conditions of the Creative Commons Attribution (CC BY) license (<https://creativecommons.org/licenses/by/4.0/>).

1. Introduction

Tracing technology has been applied in the oil and gas industry for over 70 years. Materials used in the tracing technology include isotopes [1], dyes [2,3], chemical tracers, microelements [4], ions [5], nanoparticles [6], and gases, such as noble gases [7].

They are used as monitoring and surveillance tools along with other methods, such as monitoring the production rate of reservoir fluids and using 4D seismic tests, to obtain information about reservoirs [8]. Tracers provide very informative data, especially in the complex reservoirs where other techniques could be complicated to use. Obvious information available from tracers in downhole conditions includes direct proof of communication in the connected pore spaces of the reservoir, and the determination of the underground fluid's direction pathways, oil saturation, and well-to-well connectivity. To obtain a better understanding of the formation, tracers are typically added to the injection fluids, water, or gas, to track the fluid movements inside or between reservoirs. Accordingly, tracers are commonly applied for two major types of oilfield tests—inter- and single-well tracer tests [9].

A single-well tracer test (SWTT) is performed around the borehole area (up to 10 m) and involves an injection of partitioning tracer followed by its production after a certain shut-in time. During the shut-in period, the injected partitioning tracer is miscible with oil and water phases, and overcomes partial hydrolysis in the formation brine to form a secondary tracer that is miscible with only water. The differences in the arrival times of the partitioning and secondary tracers are proportional to the downhole ratios of oil and water phases. Such tests provide information on the residual oil saturation of the formation [10,11]. Additionally, the formation permeability profile along the borehole can

be estimated via the single-well tracer method through an injection of tracers and analyzing their consequent in-situ measurements. This technique can be further applied for quality control over cementing and packing operations; by doing so, we can detect well leakage and formation fractures. Examples of compounds that are used for SWTT as a partitioning tracer include esters (such as ethyl acetate, propyl formate, etc.); water tracers, including dyes and alcohols (isopropanol, methanol, tritiated water, etc.); and gases (radon, carbon dioxide, noble gases, etc.) [8].

The inter-well tracer test is performed as an injection of passive and partitioning tracers into the injection well, followed by the tracers' propagation and monitoring of their production from the production well via produced fluids sampling and characterization. The propagation of partitioning tracers progresses with chromatographic retardation due to their equilibration with water and oil phases. These tests provide information on distant (hundreds of meters) inter-well space characteristics, such as reservoir residual oil saturation, communication between wells, reservoir porosity and heterogeneity, fluid flow paths, and hydraulic fracturing efficiency. Some examples of passive tracers used for inter-well tests include water-soluble chemicals [8], such as solvents (methanol, ethanol, *n*-/*iso*-propyl alcohol, acetone); dyes (fluorescein, rhodamine); halogen and other ions (Cl^- , I^- , SCN^- , $[\text{Co}(\text{CN})_6]^{3-}$), substituted benzoic- and fluorobenzoic acids; and isotopically labeled water (HTO, D_2O , H_2^{18}O). *tert*-Butanol, 2-propanol, tritiated *n*-butanol, ^{14}C -tagged *iso*-amyl alcohol and other C_{4+} long-chained and branched alcohols can be mentioned as partitioning inter-well tracers [9]. Non-partitioning inter-well tracer tests are valuable for well connectivity and fluids flow studies, and are performed through the injection of passive tags into an injection well (one specific tracer per one well), with their consequent detection and monitoring at the observation or production well [12].

Along with conventional uses of tracing techniques for well production surveillance and fracturing monitoring, tracers can be applied for the tracking of the well's drilling progress, drilled formation characterization, and mud-logging procedures. Thus, it was reported that the addition of tracers to drilling mud allows for the estimation of the formation's water composition [13]. Moreover, barcodable polymeric nanoparticles were applied for labeling of drill cuttings at the depth of their generation to improve the lithological characterization of formation and cuttings depth assignments [5].

Efficient chemical tracers require indicators to be tracked by unique chemical compositions or properties. Thus, the identification of radioactive isotope tracers could be performed through their radioactivity via gamma-ray logging or scintillation counting; furthermore, the detection of gases, solvents, and alcohols could be performed by their standard retention times (RT) via gas chromatography (GC or GC-MS) and/or high-performance liquid chromatography (HPLC). Chemicals, such as fluorobenzoic acid derivatives, could be analyzed by fluorine-atom presence via nuclear magnetic resonance (NMR) and/or by molecular weight and RT via HPLC-MS. Ions are commonly monitored and quantified using ionic chromatography (IC); furthermore, heavy-atom- and metal-containing ions could be tracked by ICP-AES or ICP-MS. All named tracer-based well-monitoring methods require the usage of expensive equipment and often time-consuming and labor-intensive sampling, probe preparation, and analytical techniques.

The main purpose of the current work is to design easily detectable tags for drill-cuttings labeling. To develop a fast, efficient, and simple tracing method, we engineered a novel type of fluorescent tracers and aimed these tracers' applications toward on-site near-real-time well-drilling monitoring to label drill cuttings as they are made at the drill-bit face; furthermore, we desired to improve the accuracy of drill-cuttings identification upon sorting at the shale shaker to improve on-site drill-cuttings depth correlation. Knowing the simplicity and very-low detection limits of fluorescent materials, we engineered several tracers composed of carrier-matrices that were doped or covalently modified with various commercial fluorophores to determine the robustness of these tracers for harsh downhole conditions and the possibility of their visual detection by fluorescent emissions under UV light.

2. Materials and Methods

2.1. Materials

We purchased fully hydrolyzed poly(vinyl alcohol) (PVA) (M_w approx. 145,000); fluorescein isothiocyanate (FITC); fluorescein; rhodamine B; high-purity grade SiO_2 , average pore size 60 Å (52–73 Å), 70–230 mesh, 63–200 µm, for column chromatography; and HPLC-grade solvents, including methanol, propanol-2, dimethyl sulfoxide (DMSO), pyridine, tetrahydrofuran (THF), diethyl ether, from Sigma Aldrich (St. Louis, MO, USA). We purchased commercial super-absorbent polymer (SAP) based on sodium polyacrylate (Prod.# C001B1) from Orbeegun (Moscow, Russia). We purchased glutaraldehyde, 50% aqueous solution (Cat.# 00001602) from Ruschim (Moscow, Russia). We purchased chitosan (water-soluble, MW 50–80 kDa, degree of deacetylation DD 80%) from Bioprogress (Moscow, Russia). We purchased RADGLO[®] PS-11 green thermoset fluorescent pigment from Afaya (Moscow, Russia). We used all materials and solvents without further purification. We prepared all aqueous solutions with deionized water (18.2 MΩ·cm), Sartorius, Arium[®] (Göttingen, Germany).

2.2. Synthesis of FITC-Labeled Chitosan

We dissolved chitosan (300 mg, 0.19 mmol) in water (15 mL) under vigorous stirring at room temperature (RT) over ~3 h. To obtain solution, we added fluorescein isothiocyanate (FITC) (1.48 mg, 0.0038 mmol) dissolved in ethanol (25 mL) dropwise. We chose the ratio of the reacting chemicals (FITC to *d*-glucosamine residue of chitosan) to be 1:50. We performed the reaction between fluorescein isothiocyanate and chitosan for 2 h at 50 °C in the dark to prevent fluorophore from photobleaching and yielded FITC-labeled chitosan. We precipitated the product from the reaction mixture with acetone (30 mL) and recovered by centrifugation. We performed purification of the obtained product by dispersing the resulted off-white solid in acetone (30 mL), followed by centrifugation (three times). We freeze-dried the resulted precipitate to remove residual water and yield light yellow powder of fluorescein-tagged chitosan (255 mg, 85%).

2.3. Synthesis of Pigment-Loaded Chitosan-Based Hydrogel

We dissolved chitosan (460 mg, 2.86 mmol) in water (19.54 mL) under vigorous stirring at RT over 3 h. We added commercial pigment (50 mg) in powder form to the obtained solution. The mass ratio of the pigment to chitosan was 1:10. We transferred the resulted mixture to a Petri dish followed by treating with 50% aqueous glutaraldehyde (0.2 mL, 1 mmol). We dried the produced hydrogel in a vacuum oven at 50 °C overnight to yield fine powder of cross-linked chitosan (600 mg, 98%).

2.4. Synthesis of FITC-Labeled PVA

We synthesized the PVA-FITC adduct as reported by Kaneo [14]. We dissolved PVA (300 mg, 0.68 mmol) in dimethyl sulfoxide (DMSO) (8 mL) containing (50 µL, 0.63 mmol) of pyridine; then, we added solution of FITC (50 mg, 0.13 mmol) in DMSO (1 mL) and heated obtained mixture for 2 h at 95 °C in the dark (it was important to keep reaction in the dark to prevent FITC photobleaching). After 2 h, the reaction mixture cooled down to RT, and we added propanol-2 (30 mL) to remove excess of FITC into solution, and precipitate resulted in FITC-PVA adduct. We separated the solid product via centrifugation and further purified via dispersing in propanol-2 (30 mL) followed by centrifugation (three times until absence of the fluorescent signal of the supernatant solution in UV light). We transferred the resulted powder of the product to a beaker protected from light with aluminum foil and then dried in a vacuum oven at 40 °C overnight. We obtained FITC-labeled PVA as yellow powder (273 mg, 92%).

2.5. General Procedure for Preparation of Dye-Loaded Tracers (Super-Absorbent Polymer and SiO_2)

We completely dissolved fluorescent dye (fluorescein or rhodamine B) (10 mg) in water (200 mL for SAP; 20 mL for SiO_2) under vigorous stirring for 2 h at room temperature.

To the obtained solution, we added SAP (5 g) or SiO₂ (5 g) and kept the resulted mixture for 4 h at room temperature without steering to complete dye absorption into the matrix. Upon exposure to a dye solution, SAP or SiO₂ particles soaked fluorophore. We dried the resulted wet tracers over 24 h at 70 °C under vacuum 10 mbar. We obtained four batches of fluorescein (or rhodamine B)-loaded SAP (or SiO₂) with ratio of fluorophore to matrix 2 mg to 1 g.

2.6. Analytical Characterization of Obtained Materials

We registered FTIR spectra with Nicolet iS 50 Fourier transform infrared (FTIR) spectrometer (Waltham, MA, USA) using attenuated total reflection (ATR) sampling module in the range 4000–500 cm⁻¹. We calibrated the instrument before sampling against clear and dry crystal surfaces. We registered thermogravimetry curves of samples on the TA TGA 5500 instrument (TA Instruments, New Castle, DE, USA) under nitrogen atmosphere at the temperature range from 25 to 400 °C and heating rate of 10 °C/min. We performed spectrofluorometric analysis on the Horiba FluoroMax-4 spectrofluorometer (Kyoto, Japan). We calibrated the instrument over deionized water; we performed sampling of the fluorescent dyes with deionized water solutions; and we performed sampling of the solids SAP and silica with dry materials.

We performed tracer chemical stability investigations via exposure of materials from 1 day to 1 week in five laboratory conditions mimicking downhole media. Tests included treatment of tracers with pure organic solvents, such as THF, diethyl ether, and diesel, as well as exposure of tracers to aqueous brines containing salts (1): NaCl (41.041 g/L), CaCl₂ (2.384 g/L), MgCl₂ (17.645 g/L), Na₂SO₄ (6.343 g/L), NaHCO₃ (0.165 g/L); and brine (2): NaCl (150.446 g/L), CaCl₂ (69.841 g/L), MgCl₂ (20.396 g/L), Na₂SO₄ (0.518 g/L), NaHCO₃ (0.487 g/L).

3. Results and Discussions

3.1. Preparation of Tracing Materials

To engineer efficient fluorescent tracers, we utilized a combinatorial chemistry approach for the preparation and selection of the best-performing combinations of fluorophores and carrier matrices. Knowing the possibility of aggregation-caused fluorescence-quenching fluorophores [15], we proposed and fabricated several variants of fluorophore–matrix combinations that included covalent linkages between the matrix and fluorescent moiety that could be spatially tight, as well as the spatial compartmentalization of the fluorescent molecules within the cross-linked polymeric nets. Additionally, we investigated the possibility of loading fluorophores into the sorbent matrices with various ratios to estimate efficient fluorophore concentrations excluding aggregation-caused quenching.

Various matrices were studied for the trial loading of/modification with fluorophores, including silica, poly(vinyl alcohol), chitosan, and super-absorbent polymer (SAP) based on the sodium salt of poly(methyl acrylate). A number of fluorophores including fluorescein isothiocyanate, fluorescein, rhodamine B, and commercial pigments were used in the current investigation for matrices customization. Upon the development of the tracers, we chose two different approaches of matrix modification: the covalent binding of the fluorescent agents and the physical absorption of fluorophores into the carrier to result in fluorescence-bearing tags. These fluorescent-labeled/loaded tracers were subsequently used for chemical stability evaluations and fluorescence studies.

For the development of tracers by carrier modifications through a physical absorption, selected matrices (silica and sodium polyacrylate SAP) were soaked with an aqueous solution of fluorescent dyes (fluorescein, rhodamine B, and commercial pigments), followed by the drying of the resulted impregnated sorbents in a vacuum oven. Super-absorbent polymer was used as a matrix for tracers loaded with xanthene dyes—fluorescein and rhodamine B. Similarly, a SiO₂ matrix was impregnated with fluorescein and fluorescent pigment.

To evaluate the efficiency of the chemical modification of the matrices, we chose readily available commercial polymers, such as chitosan and poly(vinyl alcohol), for treatment with fluorescein isothiocyanate. The FITC–chitosan adduct produced with a 50:1 molar

ratio of the fluorophore-to-matrix loading (Figure 1) exhibited a low intensity of fluorescent emission in the powder form and a high fluorescent emission in an aqueous solution, presumably due to the aggregation-caused fluorescent quenching [16] at the solid state.

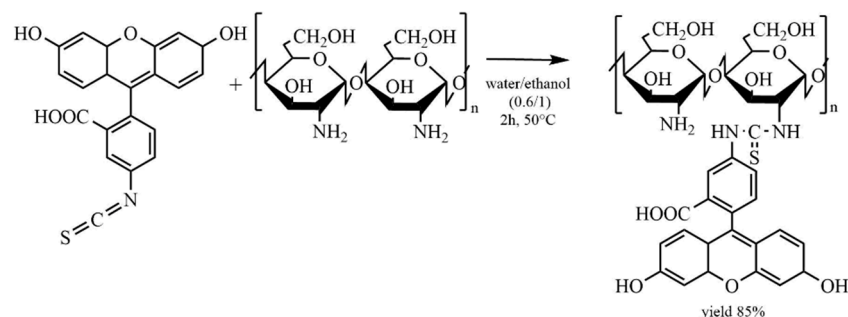


Figure 1. Synthesis of chitosan labeled with FITC.

To overcome this drawback and produce an emissive tracer, tags based on chitosan loaded with 10 wt.% of fluorescent pigment and cross-linked with glutaraldehyde were synthesized (Figure 2). The obtained cross-linked chitosan-network-bearing pigment demonstrated high fluorescent intensity, which was visible by the naked eye, both in the powder form and in aqueous suspensions.

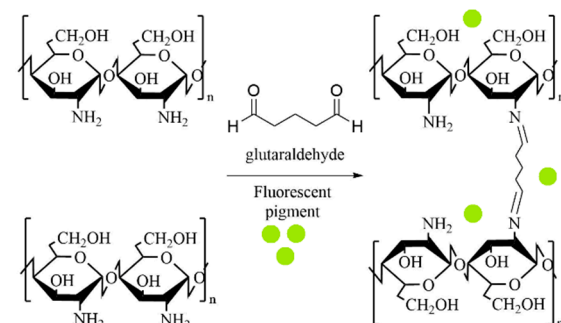


Figure 2. Synthesis of chitosan loaded with fluorescent pigment cross-linked with glutaraldehyde.

Poly(vinyl alcohol) was modified with fluorescein isothiocyanate at a molar ratio of ~5:1 according to the published procedure [15] (Figure 3). Contrary to FITC–chitosan derivatives, the FITC–PVA adduct exhibited a high fluorescent intensity upon exposure to UV light, both in dry states and in aqueous dispersions. Unfortunately, this labeled polymer has low resistance to high temperatures and brines.

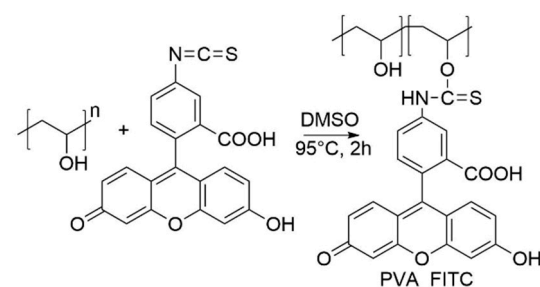


Figure 3. Synthesis of poly(vinyl alcohol)–FITC adduct.

3.2. ATR-FTIR Characterization of Tracing Materials

All engineered tracing materials were characterized using ATR-FTIR spectroscopy to elucidate the molecular structure of products modified via fluorophores loading or covalent attachment.

3.2.1. ATR-FTIR Investigations of Chitosan-Based Tracers

The FTIR spectra of chitosan-based tracers are represented in Figure 4. The FTIR spectrum of starting chitosan shows a broad absorption band at 3451 cm^{-1} , attributed to O-H stretching vibrations, which overlaps the N-H stretching at the same region. Bands at $2931\text{--}2925\text{ cm}^{-1}$ represent C-H stretching vibrations of aliphatic CH bonds of polysaccharide cycles and methylene groups. The band at 1635 cm^{-1} represents the N-H bending vibration. The bands at 1167 cm^{-1} and 1045 cm^{-1} are attributed to C-O-C stretching vibrations of the glycoside link and chitosan ring.

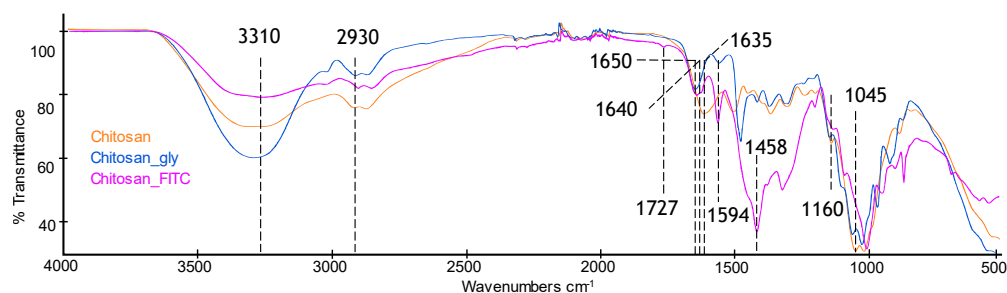


Figure 4. ATR-FT-IR spectra of chitosan (**Chitosan**); chitosan cross-linked with glutaraldehyde (**Chitosan_Gly**); and chitosan-FITC adduct (**Chitosan_FITC**).

Similarly, the FTIR spectrum of the hydrogel based on chitosan cross-linked with glutaraldehyde exhibits broad absorption bands at 3417 cm^{-1} , representing overlapping O-H and N-H stretching vibrations; furthermore, bands at $2930\text{--}2925\text{ cm}^{-1}$ are attributed to the C-H vibrations of the CH and methylene groups. Absorption bands at 1167 cm^{-1} and 1028 cm^{-1} are attributed to the C-O-C bond vibrations of the glycoside link and chitosan ring. Contrary to the starting material, the N-H bending vibration band of the amine group at $\sim 1630\text{ cm}^{-1}$ diminished in intensity, and an additional band attributed to the C=N vibrations of the imine group [17] appeared at 1652 cm^{-1} , confirming the formation of cross-linked structures upon the reaction of the chitosan amino group with glutaraldehyde.

Elucidating the structure of the FITC-chitosan adduct, we noted characteristic bands at 3417 cm^{-1} attributed to O-H and N-H stretching vibrations, and absorption bands at $2930\text{--}2925\text{ cm}^{-1}$, which were attributed to the C-H vibrations. Moreover, additional absorption peaks appeared at 1594 cm^{-1} , 1535 cm^{-1} , and 1458 cm^{-1} , which are representative of the stretching vibrations of C=C bonds in the aromatic rings of the FITC moiety. Noticeably, an additional N-H bending vibration band appeared at 1640 cm^{-1} , compared to and in addition to the amine group's bending vibration of pure chitosan at 1630 cm^{-1} , confirming the partial modification of the NH_2 residue. A small band from the lactone carbonyl group appeared at 1727 cm^{-1} , which was attributed to lactone forming the FITC moiety. The strong band at 1050 cm^{-1} can be attributed to C=S group vibrations formed upon the covalent attachment of the fluorescein isothiocyanate group to the chitosan amino function.

3.2.2. ATR-FTIR Spectroscopy of Poly(Vinyl Alcohol)-Based Tracers

To confirm the chemical modification of PVA with FITC, we registered the FTIR spectra of the starting polymer, fluorescent dye, and resulted FITC-PVA product (Figure 5). The ATR-FTIR spectrum of pure FITC demonstrates a strong absorbance peak at 2015 cm^{-1} , which is characteristic of the isothiocyanate functional group. Absorption peaks at 1594 cm^{-1} , 1535 cm^{-1} , and 1458 cm^{-1} are representative of the stretching vibrations of the C=C bonds of aromatic cycles. A comparison of the spectra of the PVA-FITC adduct and pure FITC shows the absence of absorption at 2015 cm^{-1} and indicates that isothiocyanate was fully converted upon the modification of poly(vinyl alcohol). The spectra B and C (Figure 5) show strong broad absorbance bands at 3288 cm^{-1} for pure PVA, and 3318 cm^{-1} for the FITC-labeled derivate. These bands are assigned to the O-H stretching vibrations of the hydroxyl group of PVA, and this band shows a reduced intensity in the FITC adduct

of PVA, confirming that the hydroxyl group was involved in the addition reaction with isothiocyanate. Bands corresponding to the C-H asymmetric stretching vibrations of the CH₂ group occur at 2938 cm⁻¹ and 2941 cm⁻¹, both for the starting polymer and for FITC-modified PVA. The sharp band 1087 cm⁻¹ corresponds to the C-O stretching of the secondary alcohol groups present on the PVA and FITC-PVA derivatives; furthermore, an additional absorbance band appeared in the spectrum of the FITC-modified PVA at 1013 cm⁻¹, which was attributed to the newly formed C=S bond of the FITC adduct.

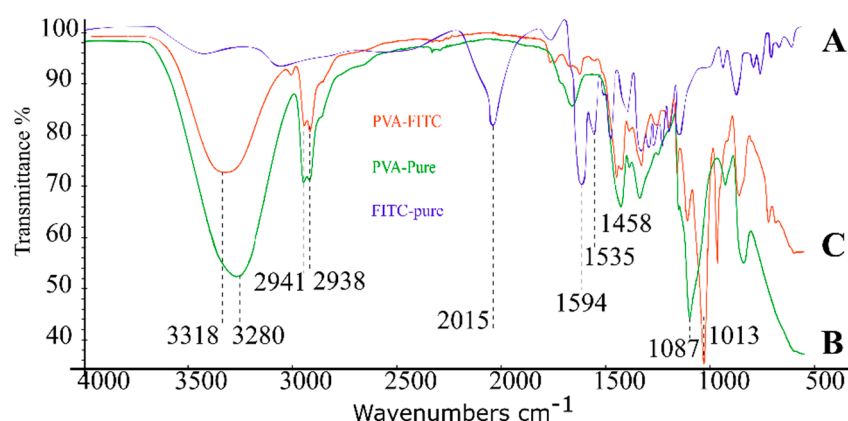


Figure 5. ATR-FTIR spectra of fluorescein isothiocyanate (A, FITC-pure); poly(vinyl alcohol) (B, PVA-pure); and FITC-PVA adduct (C, PVA-FITC).

3.2.3. ATR-FTIR Characterization of Sodium Polyacrylate-Based Tracers

The FT-IR spectra of the tracers based on sodium polyacrylate before and after loading fluorescent dyes are represented in Figure 6. The spectrum of pristine SAP exhibits a strong broad absorption area around 3400–3100 cm⁻¹, which corresponds to the stretching vibrations of the hydroxyl groups from adsorbed water. Shoulder bands around 2800 cm⁻¹ are attributed to the C-H asymmetric stretching vibrations of polymeric-chained CH and CH₂ groups. A characteristic absorption band at 1650 cm⁻¹ is attributed to the deformation vibrations of the C-OH group. Bands at 1530 cm⁻¹ and 1310 cm⁻¹ are typical for salts of carboxylic acids [18] and are attributed to the symmetrical stretching vibrations of carboxyl anions -COO⁻. Upon impregnation of the SAP sorbent with xanthene dyes, the novel bands appear at 1750 cm⁻¹, which is attributed to the -C=O vibrations of the carbonyl fragment of the lactone form of fluorescein and rhodamine B.

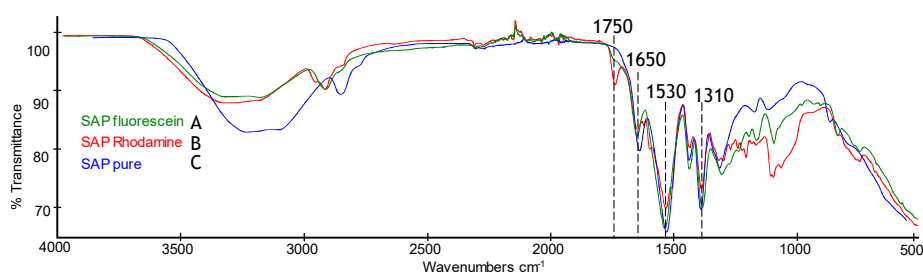


Figure 6. ATR-FT-IR spectra of pristine sodium polyacrylate (SAP pure); sodium polyacrylate loaded with fluorescein (SAP-fluorescein); and sodium polyacrylate loaded with rhodamine B (SAP-rhodamine).

Presumably, the adsorption of dyes as fluorescein and rhodamine B into the SAP matrix is associated with electrostatic acid-base interactions between the guest dye molecule and polar functional groups of the carrier matrix. At a steady state, the equilibrium between the acid and base forms of the dye will be reached, and both spirolactone and opened dye structures will be presented in the matrix. Tautomeric forms of lactone rhodamine B base and opened rhodamine B acid are represented in Figure 7.

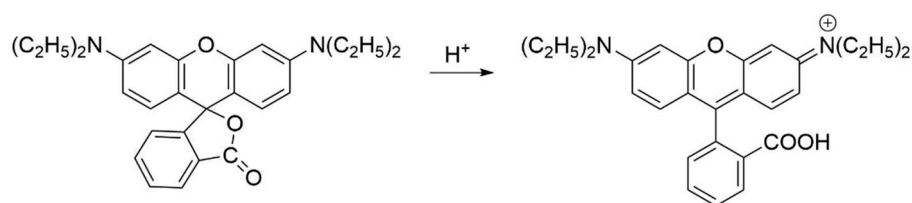


Figure 7. Acid–base equilibrium in rhodamine B forms.

3.2.4. ATR-FTIR Spectra of Silica-Based Tracers

We examined the loading of the silica-based matrix with xanthene dyes and presented the FTIR spectra of the pure and fluorescein-loaded SiO_2 in the range of $4000\text{--}500\text{ cm}^{-1}$ in Figure 8. Both spectra exhibited characteristic peaks for silica at 800 , 980 , and 1085 cm^{-1} owing to Si-O-Si symmetric stretching, Si-OH stretching, and Si-O-Si asymmetric stretching vibrations, respectively [19]. Due to the low molar ratio of SiO_2 to fluorescein, there were almost no detectable differences in the spectra of the initial and dye-loaded samples. Other than that, the porosity and non-transparent structures of the matrix can impede the detection of dye inside SiO_2 -based tracers by ATR-FTIR. The successful loading of silica with fluorescein was confirmed via UV–Vis fluorescence spectroscopy.

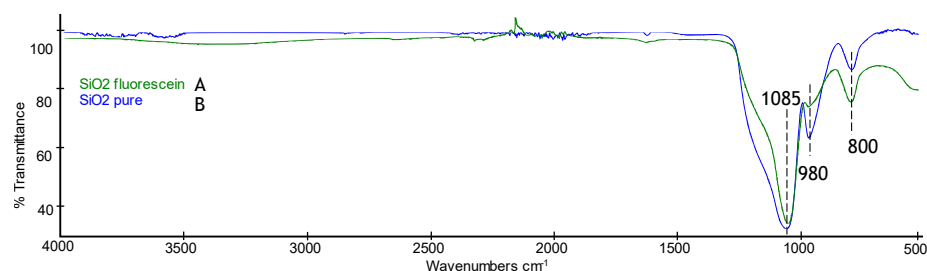


Figure 8. ATR–FTIR spectra of pure silica (SiO_2 pure) and silica loaded with fluorescein (SiO_2 fluorescein).

3.3. Chemical Stability Examination of Tracers

For the application of engineered tracers for downhole operations, we screened obtained materials for their chemical stabilities to sour media, and treated them with formation fluids. For this goal, tracer samples were exposed to acidic aqueous solutions with $\text{pH}\sim 1$. Chitosan-based materials exhibited fast degradation upon acid treatment and were detached from further tests as chemically unstable tracer carriers.

The remaining materials were further tested for stability to the conditions mimicking downhole media. Thus, samples of fluorescent-loaded tags were incubated at $90\text{ }^\circ\text{C}$ with aqueous brines containing formation salts NaCl , CaCl_2 , MgCl_2 , Na_2SO_4 , and NaHCO_3 for a period of 1 day up to 1 week. Degradation via hydrolysis was noted for fluorescent-modified poly(vinyl alcohol) upon exposure to electrolyte solutions over a few hours. Fluorescein and fluorescent-pigments-loaded silica (Flu-SiO_2), as well as xanthene-dyes-loaded super-absorbing polymer (Flu-SAP), exhibited no visible decomposition and demonstrated almost no leakage of dyes at the described conditions. Consequently, these stable matrices (Flu-SiO_2 , Flu-SAP) were further tested for resistance to organic solvents (THF, ether, and diesel). Among the materials tested for exposure to organic media, fluorescein- and rhodamine B-loaded SAPs, fluorescein, and pigments-loaded SiO_2 exhibited no visible deterioration of their fluorescent properties. Table 1 summarizes the results of these investigations.

Table 1. Examination of the chemical stability of selected tracers.

	Time	90 °C Brine 1	90 °C Brine 2	THF	Ether	Diesel
Fluorescent dye SiO ₂	One day	Stable	Stable	Stable	Stable	Stable
	One week	Stable	Stable	Stable	Stable	Stable
Fluorescein SiO ₂	One day	Stable	Stable	Stable	Stable	Stable
	One week	Stable	Stable	Reduce	Stable	Reduce
SAP loaded with fluorescein	One day	Stable	Stable	Stable	Stable	Stable
	One week	Stable	Stable	Stable	Stable	Stable
SAP loaded with rhodamine B	One day	Stable	Stable	Stable	Stable	Stable
	One week	Stable	Stable	Stable	Stable	Stable

3.4. Investigation of the Thermal Stability of Tracers by TGA

To evaluate the thermal stability of the selected tracers, we performed a TGA monitoring of the samples' weight losses upon heat treatment from RT to 400 °C at a heating rate of 10 °C/min in a nitrogen atmosphere. As shown in Figure 9a, the TG curves of silica-based tracers, as well as the pure silica, exhibited weight losses of about 5 wt. % upon exposure to 100 °C temperatures; further they kept almost a constant mass. All curves in Figure 9a demonstrated similar behaviors; moreover, the highest weight losses occurred at the temperature range of 20–150 °C and corresponded to the loss of absorbed water. Figure 9b represents the TG curves of super-absorbent-based tracers. The total gradual weight losses of the SAP-tracers at the temperature range of 20 to 400 °C reached up to 22–23%. A sharp inflection could be noted at 315 °C, which is attributed to the degradation of dyes.

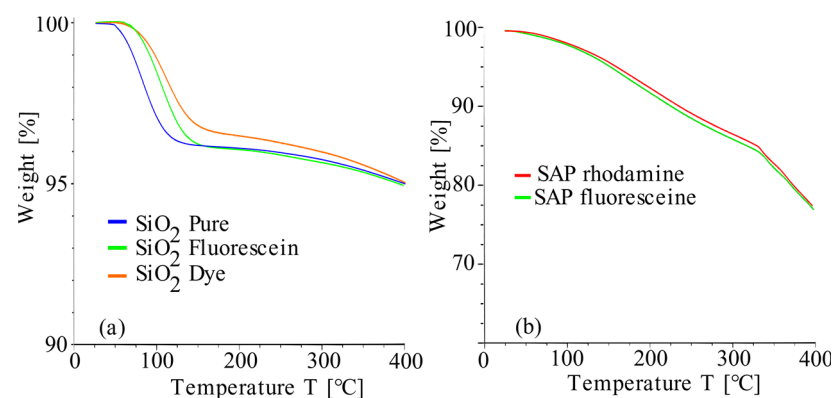


Figure 9. TGA curves: (a) SiO₂ pure, SiO₂–fluorescein, SiO₂–fluorescent pigment; and (b) SAP–fluorescein, SAP–rhodamine B.

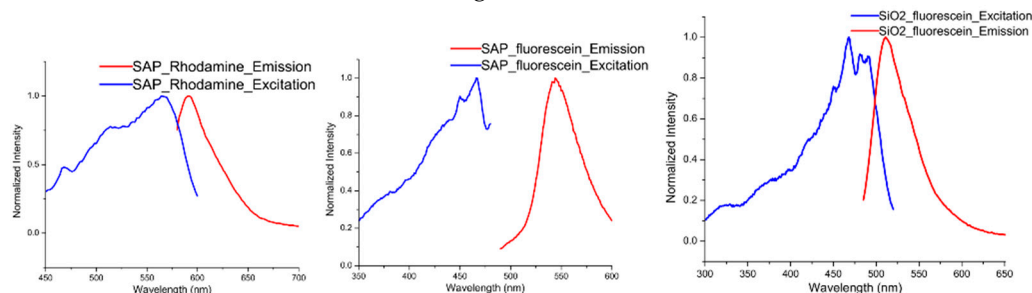
Table 2 summarizes TG total weight losses of selected tracers and indicates limits of the thermal stability of chosen specimens. Thus, tracers based on super-absorbent polymers loaded with xanthene dyes are relatively stable up to 170 °C, showing no deterioration of fluorescent properties. Silica-based tracers are even more robust during high temperature exposure.

Table 2. Evaluation of the thermal stability of selected tracers.

Type of Tracers	T _{5%} [°C]	Yield (wt. %)
SAP rhodamine B	170	78
SAP fluorescein	168	77
SiO ₂ pure	400	95
SiO ₂ fluorescein	400	95
SiO ₂ rhodamine B	400	95

3.5. Fluorescence Spectroscopy Characterization of Selected Stable Tracers

The fluorescent behaviors of fluorescein- and rhodamine B-loaded tracers were explored using UV–Vis fluorescence spectroscopy. Excitation and emission wavelengths were recorded for SAP–rhodamine B-, SAP–fluorescein-, and silica–fluorescein-loaded tracers and compared with published data because the photochemical properties of xanthene dyes are sensitive to the measurements medium [20]. Tracers based on SAP–rhodamine B demonstrated standard maxima excitation and emission wavelengths (λ_{Ex} 560 nm; λ_{Em} 590 nm) characteristic of rhodamine B (λ_{Ex} 554 nm, λ_{Em} 578 nm, [20]) without much deviation because of the interactions of the dye with the matrix. Similarly, tracers based on silica loaded with fluorescein demonstrated excitation and emission wavelengths (few peaks at λ_{Ex} 470–491 nm; λ_{Em} 515 nm) corresponding to the literature [21] (λ_{Ex} 488 nm; λ_{Em} 515 nm). Deviation from the standard values was detected only for SAP loaded with fluorescein (λ_{Ex} 462 nm; λ_{Em} = 545 nm), presumably due to the basic pH of the sodium polyacrylate matrix. Figure 10 summarizes the emission and excitation spectra for SAP and SiO₂ matrices loaded with fluorescent agents.

**Figure 10.** Fluorescence spectroscopy characterization of tracers.

3.6. Applications of Tracers in Drill-Cuttings Tagging

Selected fluorescent tracers stable to downhole conditions, namely, SAP–fluorescein-, SAP–rhodamine B-, and silica–fluorescein-loaded tags, were tested for their ability to label drill cuttings with further camera detection in laboratory conditions. For this goal, samples of the drilling cuts were collected from the oil fields and mixed with the selected tracer, and pictures of the tagged cuts under day and UV light were recorded via camera (Figure 11).

The library of pictures of tagged drilling cuts is further used for the development of an image recognition system. It is noted that tracers based on silica–fluorescein were barely detectable by the camera as a separate particle, both at day and UV light, due to their small sizes of 60–200 μm ; however, SAP-dyes-loaded tags of 0.5–1 mm in size were detectable with a camera under UV light upon drill-cuttings labeling. These obtained SAP-based tracers were clearly visible after mixing with drill-cuttings samples, especially under UV light. This type of tag is primary selected for drill cuttings colored tagging according to the depth of the mud-cuttings on circulation prototype equipped with the shale shaker and UV camera. Recorded photographs and videos of tagged formation cuts are used for the further engineering of camera-detection- and AI-based image recognition systems, and consequent field trials are currently ongoing.

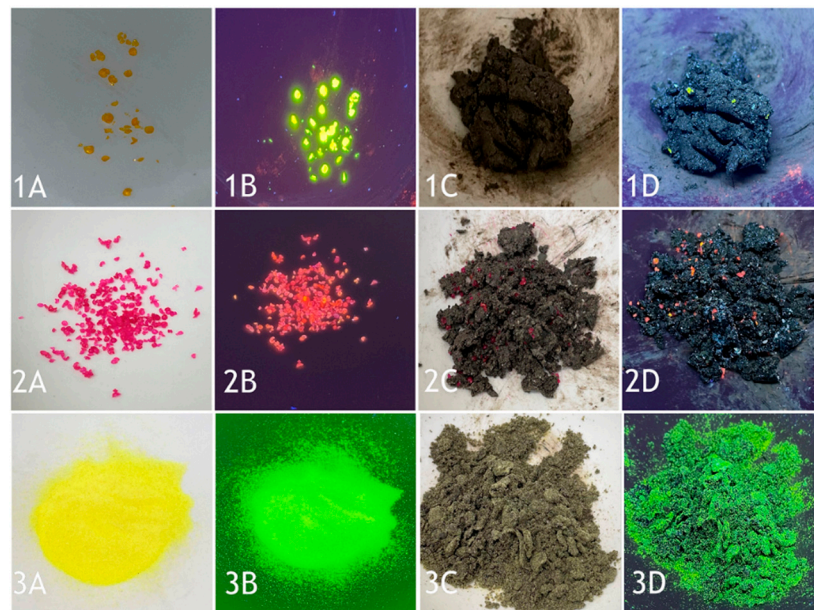


Figure 11. Examples of pictures for tracers' labeling of drill cuttings. (1A)—SAP-fluorescein tags at day light; (1B)—SAP-fluorescein tags at UV light; (1C)—drill cuttings tagged with SAP-fluorescein tags at day light; (1D)—drill cuttings tagged with SAP-fluorescein tags at UV light. (2A)—SAP-rhodamine B tags at day light; (2B)—SAP-rhodamine B tags at UV light; (2C)—drill cuttings tagged with SAP-rhodamine B tags at day light; (2D)—drill cuttings tagged with SAP-rhodamine B tags at UV light. (3A)—Silica-fluorescein tags at day light; (3B)—silica-fluorescein tags at UV light; (3C)—drill cuttings tagged with silica-fluorescein tags at day light; (3D)—drill cuttings tagged with silica-fluorescein tags at UV light.

4. Conclusions

In the present study, we demonstrated the design and preparation of a variety of cost-efficient and readily available fluorescent tags composed of carrier-matrices loaded with/covalently modified fluorophores. This novel engineered library of tracers was screened at various harsh medias to select stable fluorescent particles resistant to the conditions mimicking the downhole environment. The most-stable obtained materials exhibited high chemical stability and thermal robustness up to temperatures of 170 °C and above. Based on these data, it is proven that prepared tracers can be used in downhole applications. The prepared fluorescent-loaded tags are suitable for downhole tests for labeling of drill cuttings accompanied by the detection of tagged cuttings for drilling depth assignment via well-head camera on shale shaker.

Thus, we innovated a fast and efficient method for downhole fluorescent drill cuttings tracing developed for on-site near-real-time detection with a UV camera and image-recognition system. The fast and simple determination of drill-cuttings depth would improve the accuracy of drilling depth correlation and advance the petrophysical characterization of formations, allowing for optimal well placement.

5. Patents

The materials presented in this work and their proposed applications are covered by IP.

Author Contributions: Conceptualization, N.A. and V.S.; methodology, V.K.; formal analysis, V.K.; investigation, V.K. and V.S.; resources, N.A., V.K. and V.S.; writing—original draft preparation, V.K. and V.S.; writing—review and editing, N.A.; supervision, V.S.; project administration, V.S.; funding acquisition, V.S. All authors have read and agreed to the published version of the manuscript.

Funding: This research received no external funding.

Institutional Review Board Statement: Not applicable.

Informed Consent Statement: Not applicable.

Data Availability Statement: Exclude, this study did not report any data.

Conflicts of Interest: The authors declare no conflict of interest.

References

1. Ciszkowski, C.; Ouled Ameer, Z.; Forsyth, J.P.J.; Nightingale, M.; Shevalier, M.; Mayer, B. Application of Geochemical and Isotopic Tracers for Characterization of SAGD Waters in the Alberta Oil-Sand Region. *SPE Prod. Oper.* **2020**, *35*, 188–201. [\[CrossRef\]](#)
2. Hemed, T.S. Development of a Tracer Analysis System Using Dye Tracers. In Proceedings of the SPE Annual Technical Conference and Exhibition, Virtual Event, 26–29 October 2020. [\[CrossRef\]](#)
3. Green, L.; Entzminger, D.; Tovar, D.; Alimahomed, A.; Alimahomed, F.; Defeu, C.; Malpani, R. Tying Horizontal Measurements to Well Performance Using Production Logs and Chemical Tracers in Multiple Wolfcamp Shale Wells, Delaware Basin. In Proceedings of the Society of Petroleum Engineers—SPE Hydraulic Fracturing Technology Conference and Exhibition 2019, The Woodlands, TX, USA, 5–7 February 2019. [\[CrossRef\]](#)
4. Li, J.; Jiang, H.; Liu, Y. Investigation of Pore-Scale Dispersion in Polymer Flooding. In Proceedings of the Society of Petroleum Engineers—International Petroleum Technology Conference 2011, Bangkok, Thailand, 15–17 November 2011. [\[CrossRef\]](#)
5. Hall, C.; Hughes, T.L. Ion Chromatography Tracer Experiments During Drilling. In Proceedings of the SPE International Symposium on Oilfield Chemistry, New Orleans, LA, USA, 2–5 March 1993. [\[CrossRef\]](#)
6. Antoniv, M.; Sherry Zhu, S.; Chang, S.; Poitzsch, M.E.; Jabri, N.M.; Marsala, A.; O'Brien, J. Method for Detecting Nanoparticles on Cuttings Recovered from a Gas Reservoir. *Energy Fuels* **2021**, *35*, 7708–7716. [\[CrossRef\]](#)
7. Khan, M.N.; Iwama, H.; Al-Neaimi, A.; Al-Shehhi, O.; Chatterjee, M. A to Z of Gas Tracers—A Decade of Learning and Experience. In Proceedings of the Society of Petroleum Engineers—Abu Dhabi International Petroleum Exhibition and Conference, Abu Dhabi, UAE, 7–10 November 2016. [\[CrossRef\]](#)
8. Serres-Piole, C.; Preud'homme, H.; Moradi-Tehrani, N.; Allanic, C.; Jullia, H.; Lobinski, R. Water Tracers in Oilfield Applications: Guidelines. *J. Pet. Sci. Eng.* **2012**, *98–99*, 22–39. [\[CrossRef\]](#)
9. Anisimov, L.A.; Kilyakov, V.N.; Vorontsova, I.V. The Use of Tracers for Reservoir Characterization. In Proceedings of the SPE Middle East Oil and Gas Show and Conference (MEOS), Manama, Bahrain, 15–18 March 2009. [\[CrossRef\]](#)
10. Tomich, J.F.; Dalton, R.L.; Deans, H.A.; Shallenberger, L.K. Single-Well Tracer Method to Measure Residual Oil Saturation. *J. Pet. Technol.* **1973**, *25*, 211–218. [\[CrossRef\]](#)
11. Khaledialidusti, R.; Kleppe, J.; Enayatpour, S. Evaluation and Comparison of Available Tracer Methods for Determining Residual Oil Saturation and Developing an Innovative Single Well Tracer Technique: Dual Salinity Tracer. In Proceedings of the International Petroleum Technology Conference, Kuala Lumpur, Malaysia, 10–12 December 2014. [\[CrossRef\]](#)
12. Al-Murayri, M.T.; Al-Qenae, A.; AlRukaibi, D.; Chatterjee, M.; Hewitt, P. Design of a Partitioning Interwell Tracer Test for a Chemical EOR Pilot Targeting the Sabriyah Maaddud Carbonate Reservoir in Kuwait. In Proceedings of the Society of Petroleum Engineers—SPE Kuwait Oil and Gas Show and Conference, Kuwait City, Kuwait, 15–18 October 2017. [\[CrossRef\]](#)
13. McCartney, R.A.; de LG Solbe, M.J. Use of Tracers in Drilling Muds to Allow the Estimation of In-Situ Formation Water Compositions From Drilling-Mud-Contaminated Formation Water Samples. In Proceedings of the SPE International Symposium on Oilfield Chemistry, Houston, TX, USA, 16–19 February 1999. [\[CrossRef\]](#)
14. Kaneo, Y.; Hashihama, S.; Kakinoki, A.; Tanaka, T.; Nakano, T.; Ikeda, Y. Pharmacokinetics and Biodisposition of Poly(Vinyl Alcohol) in Rats and Mice. *Drug Metab. Pharmacokinet.* **2005**, *20*, 435–442. [\[CrossRef\]](#) [\[PubMed\]](#)
15. Tang, Y.; Tang, B.Z. *Handbook of Aggregation-Induced Emission, Volume 1: Tutorial Lectures and Mechanism Studies*; John Wiley & Sons Inc.: Hoboken, NJ, USA, 2022; p. 496.
16. Chen, S.; Wang, H.; Hong, Y.; Tang, B.Z. Fabrication of Fluorescent Nanoparticles Based on AIE Luminogens (AIE Dots) and Their Applications in Bioimaging. *Mater. Horiz.* **2016**, *3*, 283–293. [\[CrossRef\]](#)
17. Triana-Guzmán, V.L.; Ruiz-Cruz, Y.; Romero-Peñaloza, E.L.; Zuluaga-Corrales, H.F.; Chaur-Valencia, M.N. New Chitosan-Imine Derivatives: From Green Chemistry to Removal of Heavy Metals from Water. *Rev. Fac. De Ing. Univ. De Antioq.* **2018**, *89*, 34–43. [\[CrossRef\]](#)
18. Grabowska, B.; Holtzer, M. Structural Examination of the Cross-Linking Reaction Mechanism of Polyacrylate Binding Agents. *Arch. Metall. Mater.* **2009**, *54*, 427–437.
19. Yadav, A.K.; Singh, P. A Review of the Structures of Oxide Glasses by Raman Spectroscopy. *RSC Adv.* **2015**, *5*, 67583–67609. [\[CrossRef\]](#)
20. Kathiravan, A.; Anbazhagan, V.; Jhonsi, M.A.; Renganathan, R. Fluorescence Quenching of Xanthene Dyes by TiO₂. *Z. Fur Phys. Chem.* **2007**, *221*, 941–948. [\[CrossRef\]](#)
21. Sjöback, R.; Nygren, J.; Kubista, M. Absorption and Fluorescence Properties of Fluorescein. *Spectrochim. Acta Part A Mol. Biomol. Spectrosc.* **1995**, *51*, L7–L21. [\[CrossRef\]](#)